Chang *et al.*
Terrestrial, Atmospheric and Oceanic Sciences (2023) 34:7
https://doi.org/10.1007/s44195-023-00040-8

Terrestrial, Atmospheric and Oceanic Sciences

ORIGINAL ARTICLE

Open Access

Quantifying the probability and uncertainty of multiple-structure rupture for Taiwan

Chieh-Chen Chang[1], Chih-Yu Chang[1], Jia-Cian Gao[2] and Chung-Han Chan[1,2*]

Abstract

This study identifies structure pairs with the potential for simultaneous rupture in a coseismic period and quantifies their rupture recurrence intervals. To assess the potential for a multiple-structure rupture, we calculated the probability of Coulomb stress triggering between seismogenic structures in Taiwan. We assumed that a multiple-structure rupture would occur if two structures could trigger each other by enhancing the plane with thresholds of a Coulomb stress increase and the distance between the structures and identified various sets of seismogenic structure pairs accordingly. We discussed the uncertainty of multiple-structure pair identification from various thresholds of stress change and structure distances, effective friction coefficient, and rotation of rake angles. To estimate the recurrence intervals for multiple-structure ruptures, we implemented a scaling law and the Gutenberg-Richter law in which the slip rate could be partitioned based on the magnitudes of the individual structure and multiple-structure ruptures. Considering that one structure may be involved in multiple cases of multiple-structure ruptures, we developed new formulas for slip partitioning in a complex fault system. By implementing the range of rupture area and slip rate of each structure, the magnitudes and recurrence intervals of multiple-structure ruptures could be estimated. We discussed the epistemic uncertainties of recurrence interval from deviations of slip rate and rupture area, various empirical formula of rupture parameters. The multiple-structure rupture with a larger characteristic magnitude would be crucial for the safety evaluation of infrastructures.

Key points

1. Multiple-structure rupture could cause an earthquake with a larger magnitude.
2. We indicate cases of multiple-structure rupture and their recurrence intervals.
3. Our outcomes are crucial for safety evaluation considering a long return period.

Keywords Multiple-structure rupture, Coulomb stress change, Scaling law, Gutenberg-Richter law, Taiwan

1 Introduction

A rupture taking place along several fault segments and/or structures can cause an earthquake with a large magnitude (e.g., Yen and Ma 2011) and often leads to disaster. The 1935 M_L7.1 Hsinchu-Taichung, Taiwan, earthquake is an example. This event is attributed to a rupture on the Shihtan and Tunzijiao faults and resulted in more than 3000 fatalities and the destruction of more than 60,000 buildings. According to the fault parameters determined by Shyu et al. (2020), either the Shihtan or Tunzijiao

*Correspondence:
Chung-Han Chan
hantijun@googlemail.com
[1] Department of Earth Sciences, National Central University, Taoyuan, Taiwan
[2] Earthquake-Disaster and Risk Evaluation and Management (E-DREaM) Center, National Central University, Taoyuan, Taiwan

fault could cause an earthquake with a maximum magnitude of only 6.6 (Wang et al. 2016a). This case raises the importance of multiple-structure ruptures on seismic hazard assessment.

Thus, the Taiwan Earthquake Model (TEM) has considered the possibility of several multiple-structure ruptures for a probabilistic seismic hazard assessment for Taiwan (Chan et al. 2020) according to the finding of Shyu et al. (2020). In their procedure, however, the case that one structure could be associated with multiple pairs was determined based on geomorphological and geological evidence without detailed descriptions and possibility of the multiple-structure rupture was not discussed.

Some previous studies have quantified recurrence intervals for multiple-structure rupture. For example, Chan et al. (2020) proposed a procedure for partitioning the slip rate of each individual structure to multiple structures. The outcomes of the recurrence interval for each rupture pair have been implemented for subsequent probabilistic seismic hazard assessment (PSHA). In the study of Chan et al. (2020), however, the uncertainties contributed from different factors have not been incorporated and the case of single structure contributes to several multiple-structure ruptures is not considered. Besides, the Seismic Hazard and Earthquake Rate In Fault Systems (also known as 'SHERIFS', Chartier et al. 2017) considers multiple-fault (fault-to-fault) ruptures to evaluate seismicity rates for different magnitude (also known as 'magnitude-frequency distribution, MFD'). In the SHERIFS, fault rupture could be in the forms of not only earthquakes on a fault segment, along multiple faults, but also background seismicity taking place in the vicinity of faults. The SHERIFS provide comprehensive procedure to calculate seismicity rate on a multiple-structure system, while users need to identify cases of multiple-structure rupture by themselves before applying this system.

To identify possible pairs of multiple-structure rupture, the UCERF3 (Uniform California Earthquake Rupture Forecast, Version 3; Field et al. 2014) defines two faults that could rupture simultaneously if rupture of one fault could result in increase of Coulomb stress and the distance between the two is less than 5 km. However, the impact of thresholds of Coulomb stress change and fault distance on multiple-structure rupture pair identification hasn't been well-discussed.

Thus, this study aims to identify structures that could rupture simultaneously and propose a set of formulas to evaluate their recurrence intervals based on physics- and statistics-based models. The possibility of a multiple-structure rupture is determined based on the Coulomb stress change imparted by each structure and the distance from one to the other. Quantifying the recurrence interval relies on a scaling law and the Gutenberg-Richter law (Gutenberg and Richter 1944). We quantify uncertainties of multiple-structure rupture pair identifications and recurrence intervals considering different triggering criteria and epistemic uncertainties. In addition, the impact of multiple-structure rupture on subsequent probabilistic seismic hazard assessment is also discussed. Our approach is transparent and can be applied to reexamining the composite ruptures of the seismogenic structure system in Taiwan and other regions, which is beneficial to subsequent probabilistic seismic hazard assessments.

2 Distinguishing possible seismogenic structure pairs according to Coulomb stress change

Previous studies (e.g., Catalli and Chan 2012) have concluded that changes in the Coulomb stress resulting from previous earthquakes could trigger the occurrence of subsequent events in adjacent areas. Such an approach would be especially applicable to determining the interaction between two structures if their rupture mechanisms are known so that source rupture and receiver plane for Coulomb stress calculation can be determined. We introduce the Coulomb failure criterion to discuss interaction between structure systems, then distinguish seismogenic structure pairs that could rupture together in a coseismic period, considering different criteria. The procedure of our approach is illustrated by a flow chart (Fig. 1) and detailed in the following.

2.1 Introduction of Coulomb stress

The Coulomb failure criterion describes mainly the characteristics of material failure (King et al. 1994; Toda et al. 2011). The criterion illustrates a plane encountering stress change, which could be decomposed into two vectors, shear stress change, $\Delta\tau$, and normal stress, $\Delta\sigma_n$:

$$\Delta CFS = \Delta\tau - \mu\prime\Delta\sigma_n, \tag{1}$$

where ΔCFS is the Coulomb stress change, and μ' is the effective friction coefficient that varies for different tectonic regimes. We first assume an intermediate value of $\mu' = 0.4$ then discuss its impact on the analysis. This study used the COULOMB 3.4 software (Toda et al. 2011) for calculation of Coulomb stress change. Based on the Coulomb stress change, we could quantify the possibility of a coseismic rupture for two faults. To explore the interactions between seismogenic structures in Taiwan, detailed structural parameters should be considered. Note that since we implemented a static Coulomb stress change to evaluate possibility of multiple-structure rupture, it

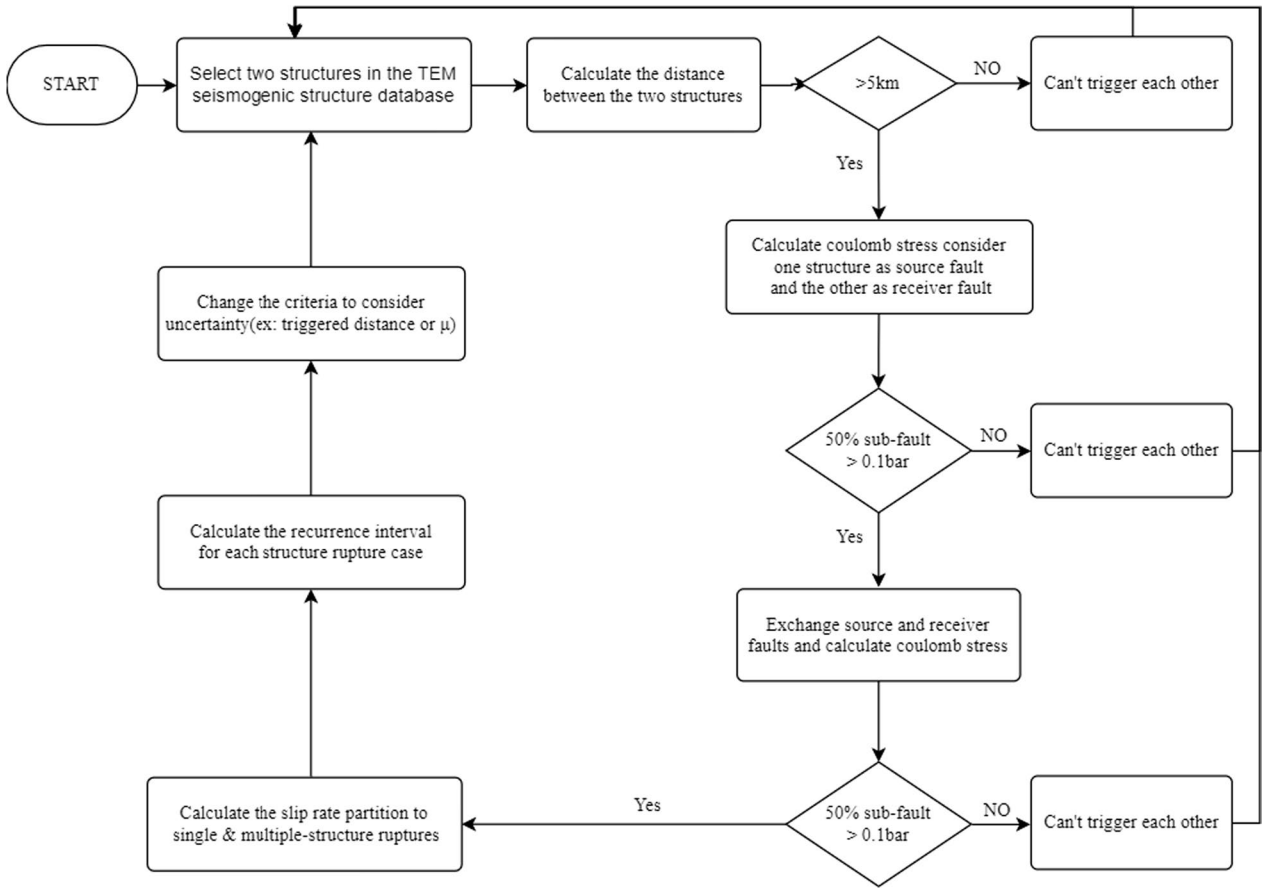

Fig. 1 A flow chart that illustrate the procedure to identify cases of multiple-structure rupture implemented in this study

is difficult to quantify the temporal evolution of rupture probability. Thus, the possibility of a multiple-structure rupture in a coseismic period might be overestimated, that is, a structure could be triggered in a postseismic or interseismic period.

2.2 Possible coseismic multiple-structure rupture defined by the Coulomb stress transfer

To understand stress interaction between seismogenic structures in Taiwan, we accessed the TEM database, which incorporates 45 seismogenic structures (Shyu et al. 2016, 2020, structure alignment shown in Fig. 2) and corresponding parameters (shown in Table 1). According to the surface trace and dipping angles, the three-dimensional geometry of each structure is illustrated by pieces of sub-faults.

Since these structures could initiate earthquakes and trigger neighboring structures, we investigated their potential interaction through Coulomb stress change. We followed the assumption of the TEM model and considered a characteristic earthquake with corresponding slip (shown in Table 1) on each structure and evaluated the Coulomb stress change solved on each sub-fault of the other structures. Previous studies concluded that stress increases greater than a threshold could trigger subsequent earthquakes. For example, Ma et al. (2005) suggested that stress increases greater than 0.1 bar could trigger seismicity activity. Thus we assumed that a structure could be triggered if more than a half of the structure's sub-faults was enhanced with a stress increase greater than the threshold of 0.1 bar. Close distance between two structures is another key factor of rupture triggering. The UCERF3 (Field et al. 2014) defines two faults that could rupture simultaneously if the distance between the two is less than 5 km. Such criterion has also been confirmed in the case of Greece defined by Chartier et al. (2017). Following the distant criteria mentioned above, we could identify seismogenic structure pairs that could rupture in a coseismic period.

We have identified seismogenic structure pairs that could rupture in a coseismic period based on the assumptions mentioned above. Initially, we set stress and distance thresholds of $\Delta CFS \geq 0.1$ and 5 km, respectively, to identify potential rupture pairs. Our

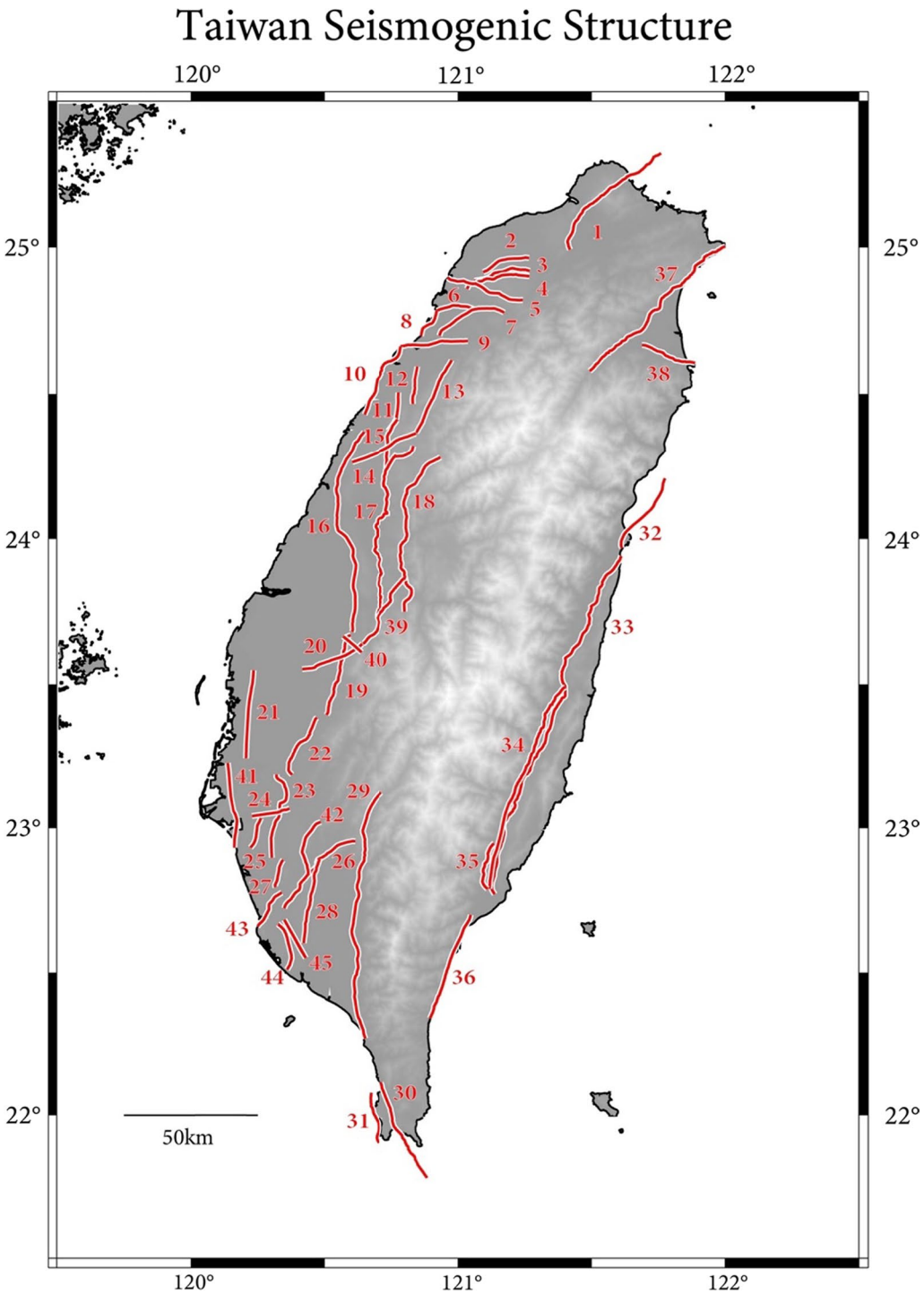

Fig. 2 Distribution of the 45 seismogenic structures in Taiwan. Corresponding structure parameters are listed in Table 1

results showed that either the Meishan fault (ID 20) or the Chiayi frontal structure (ID 21) could trigger more than 50% of the other structure's plane. For example, if the rupture initiates on the Chiayi frontal structure, the stress on the Meishan fault plane would be significantly disturbed, and 64% of the fault plane could be enhanced by more than 0.1 bar of the Coulomb stress. Conversely, a rupture on the Meishan fault could result

Table 1 The structure parameters of the 45 seismogenic structures in Taiwan

ID	Seismogenic structure	Type	Rake	Depth1	Dip1	Depth2	Dip2	Depth3	Dip3	Min area (km^2)	Mean area (km^2)	Max area (km^2)	M_w	Characteristic slip (m)	Min slip rate (mm/year)	Mean slip rate (mm/year)	Max slip rate (mm/year)
1	Shanchiao fault	N	− 90	7.0	60	10.0	45	14	30	714	1054	1732	7.01	1.29	1.1	1.7	2.9
2	Shuanglienpo structure	R	90	3.0	45	5.0	15	–	–	79	132	238	6.24	0.72	0.1	0.1	0.5
3	Yangmei structure	R	90	3.0	60	–	–	–	–	47	76	115	6.03	0.60	0.1	0.2	0.7
4	Hukou fault	R	90	10.0	30	–	–	–	–	319	512	898	6.77	1.16	0.2	0.5	2.3
5	Fengshan river strike-slip structure	LL	0	13.8	85	–	–	–	–	363	425	492	6.66	0.95	1.8	3.2	10.2
6	Hsinchu fault	R	90	10.0	45	–	–	–	–	142	205	303	6.41	0.83	0.3	0.7	2.9
7	Hsincheng fault	R	90	12.9	30	–	–	–	–	482	733	1238	6.91	1.31	0.5	1.1	5.4
8	Hsinchu frontal structure	R	90	10.0	30	–	–	–	–	151	242	425	6.48	0.90	0.6	1.4	6.8
9	Touhuanping structure	RL	180	12.0	85	–	–	–	–	258	311	367	6.52	0.80	0.1	0.1	0.1
10	Miaoli frontal structure	R	90	10.0	30	–	–	–	–	385	618	1084	6.84	1.22	0.8	1.8	8.8
11	Tunglo structure	R	90	3.5	30	–	–	–	–	61	110	207	6.17	0.68	0.2	0.5	2.6
12	East Miaoli structure	R	90	4.0	30	–	–	–	–	67	115	211	6.19	0.69	0.4	0.8	3.9
13	Shihtan fault	R	90	10.8	75	–	–	–	–	274	343	418	6.61	0.99	0.6	1.4	5.3
14	Sanyi fault	R	90	9.0	15	–	–	–	–	610	1036	1888	7.04	1.45	0.3	0.9	4.6
15	Tuntzuchiao fault	RL	180	14.8	85	–	–	–	–	345	401	460	6.64	0.94	0.3	0.5	1.7
16	Changhua fault	R	90	3.0	45	5.0	30	12	10	2036	3991	9799	7.57	2.35	1.0	1.9	7.0
17	Chelungpu fault	R	90	12.0	15	–	–	–	–	2687	4260	7409	7.60	2.45	6.9	6.9	6.9
18	Tamaopu—Shuangtung fault	R	90	6.0	30	–	–	–	–	538	830	1417	6.96	1.38	0.5	1.1	4.9
19	Chiuchiungkeng fault	R	90	12.0	30	–	–	–	–	523	806	1375	6.95	1.37	1.9	4.7	23.4
20	Meishan fault	RL	180	14.7	85	–	–	–	–	320	372	427	6.60	0.89	2.5	2.5	2.5
21	Chiayi frontal structure	R	90	12.0	15	–	–	–	–	997	1581	2749	7.21	1.71	1.4	3.4	16.1

Table 1 (continued)

ID	Seismogenic structure	Type	Rake	Depth1	Dip1	Depth2	Dip2	Depth3	Dip3	Min area (km^2)	Mean area (km^2)	Max area (km^2)	M_w	Characteristic slip (m)	Min slip rate (mm/year)	Mean slip rate (mm/year)	Max slip rate (mm/year)
22	Muchiliao—Liuchia fault	R	90	12.0	30	–	–	–	–	411	634	1081	6.85	1.23	4.4	5.8	7.1
23	Chungchou structure	R	90	12.0	30	–	–	–	–	454	701	1195	6.89	1.28	9.0	12.2	18.7
24	Hsinhua fault	RL	180	15.0	85	–	–	–	–	192	223	255	6.38	0.69	0.8	2.7	4.5
25	Houchiali fault	R	90	5.0	45	–	–	–	–	60	86	128	6.07	0.61	6.1	7.1	8.7
26	Chishan fault	LL/R	45	10.8	75	–	–	–	–	358	447	545	6.68	0.97	0.7	1.1	1.5
27	Hsiaokang-shan fault	R	90	7.0	30	–	–	–	–	104	155	260	6.30	0.75	0.8	1.8	8.0
28	Kaoping River structure	LL/R	45	12.3	75	–	–	–	–	348	425	507	6.66	0.95	0.2	0.3	1.1
29	Chaochou fault	LL/R	45	11.1	75	–	–	–	–	919	1142	1385	7.10	1.62	0.6	1.0	3.0
30	Hengchun fault	LL/R	45	15.0	75	–	–	–	–	553	651	758	6.85	1.20	5.7	6.2	6.6
31	Hengchun offshore structure	R	90	4.0	30	–	–	–	–	92	158	288	6.31	0.77	1.9	3.2	7.0
32	Milun fault	LL/R	45	10.0	75	–	–	–	–	265	337	416	6.56	0.85	9.9	10.2	10.5
33	Longitudinal Valley fault	R/LL	45	5.0	75	15.0	60	20	45	2805	3509	4676	7.52	2.25	5.6	11.4	17.1
34	Central Range structure	R	90	20.0	45	–	–	–	–	1894	2438	3307	7.38	2.00	4.8	7.3	11.2
35	Luyeh fault	R	90	2.0	45	4.0	30	–	–	90	134	223	6.24	0.71	3.6	5.3	8.0
36	Taimali coast-line structure	R/LL	45	10.6	75	–	–	–	–	373	470	574	6.73	1.10	5.7	7.3	9.0
37	Northern Ilan structure	N	–90	9.4	60	–	–	–	–	591	814	1115	6.90	1.14	1.0	3.3	6.3
38	Southern Ilan structure	N	–90	11.3	60	–	–	–	–	216	284	379	6.43	0.64	4.5	5.5	6.9
39	Chushiang structure	R/RL	135	3.0	55	–	–	–	–	44	72	112	6.00	0.57	2.0	5.0	9.0
40	Gukeng structure	LL	0	12.0	85	–	–	–	–	92	111	131	6.07	0.48	0.6	0.9	2.6
41	Tainan frontal structure	R	90	3.0	30	12.0	15	–	–	1076	1723	2964	7.24	1.74	0.5	0.9	3.5

Table 1 (continued)

ID	Seismogenic structure	Type	Rake	Depth1	Dip1	Depth2	Dip2	Depth3	Dip3	Min area (km^2)	Mean area (km^2)	Max area (km^2)	M_w	Characteristic slip (m)	Min slip rate (mm/year)	Mean slip rate (mm/year)	Max slip rate (mm/year)
42	Longchuan structure	R	90	12.0	60	–	–	–	–	246	320	422	6.58	0.96	0.9	1.7	6.5
43	Youchang sturcture	R/RL	135	12.0	75	–	–	–	–	172	206	256	6.41	0.83	0.9	1.6	5.5
44	Fengshan hills frontal structure	R	90	15.0	30	–	–	–	–	386	573	949	6.81	1.19	0.4	0.9	4.2
45	Fengshan structure	LL/R	30	15.0	85	–	–	–	–	218	253	290	6.50	1.19	10.0	10.0	10.0

The alignments of the structures are presented in Fig. 2. *LL* left-lateral strike-slip mechanism, *N* normal mechanism, *R* reverse mechanism, *RL* right-lateral strike-slip mechanism

in 76% of the Chiayi frontal structure's plane experiencing a stress increase of more than 0.1 bar.

To investigate the influence of sub-fault size on Coulomb stress analysis, we reconfigured the sub-fault geometries. Initially, we divided each sub-fault into two sections and calculated the Coulomb stress. The results showed that 64% of the Meishan fault could be triggered by the rupture on the Chiayi frontal structure, while 76% of the Chiayi frontal structure could be triggered by the Meishan fault. These findings were similar to the original analysis. Subsequently, we merged two sub-faults into one and obtained trigger probabilities of 56% and 77% for the respective cases. The subtle differences could be attributed to variations in fault geometries, which emphasize the importance of precise mechanisms for calculating Coulomb stress.

Moreover, based on the three-dimensional geometries of the two seismogenic structures, their closest distance is 1.87 km, meeting our proximity criterion (< 5 km). Therefore, we conclude that the Meishan fault and the Chiayi frontal structure can mutually induce a coseismic rupture.

Based on the procedure mentioned above, we reported the ratio by which each structure plane is triggered by other structures (Additional file 1: Table S1) and the distance between each pair of structures (Additional file 2: Table S2), we defined 17 pairs of seismogenic structures that could potentially rupture in a coseismic period (Table 2).

2.3 Uncertainties of coseismic multiple-structure rupture defined from the Coulomb stress transfer and structure distance

In addition to implementing fixed thresholds for identifying multiple-structure pairs, we further discussed the impact of different thresholds of stress changes and structure distances. Considering ΔCFS of 0.01 bar as a lower bound of stress triggering (e.g., Chan and Stein 2009; Stein 2004), we proposed four sets of stress increase thresholds (0.01, 0.05, 0.1, and 0.2 bars), as well as two threshold sets for the distance between structures (2.5 and 5.0 km). Based on the criteria, multiple-structure pairs were identified (Table 3). More structure pairs were expected if a lower ΔCFS threshold and/or a longer maximum distance were assumed and vice versa. The number of identified pairs is between 6 (ΔCFS $\geq$ 0.2 bar, distance $\leq$ 2.5 km) and 34 (ΔCFS $\geq$ 0.01 bar, distance $\leq$ 5.0 km). It should be noted that both UCERF3 (Field et al. 2014) and Chartier et al. (2019) suggested that a distance of 5 km between structures could rupture simultaneously.

We have identified potential structures that might rupture in a coseismic period. To understand the activities of these multiple-structure rupture cases, we will next propose a procedure to evaluate their recurrence intervals.

3 Recurrence interval of the multiple-structure rupture

The recurrence interval is a critical parameter in probabilistic seismic hazard analysis. Here, we are going to calculate the recurrence interval of multiple-structure ruptures and discuss their impact on seismic hazard assessment.

3.1 Recurrence interval of multiple-structure ruptures

According to the TEM seismogenic structure database (Shyu et al. 2020) and the TEM PSHA2020 (Chan et al. 2020), the rupture recurrence interval of a single seismogenic structure (L), R_L, can be evaluated as the ratio of slip of a characteristic earthquake to slip rate (denoted as D_L and $\dot{D}_L$, respectively):

$$R_L = \frac{D_L}{\dot{D}_L}. \tag{2}$$

To evaluate the seismic rate of a multiple-structure rupture on two seismogenic structures ($L1$ and $L2$), we implemented the Gutenberg-Richter law (G-R law) to describe the relationship between earthquake frequency N and magnitude M:

$$log(\boldsymbol{N}) = a - bM. \tag{3}$$

Considering the different moment magnitudes between single-structure and multiple-structure ruptures, the ratio of earthquake frequency to slip-rate partitioning could be evaluated by the G-R law. Here we present C_1 and C_2 as the partitioned rates from the first and second structures, $L1$ and $L2$, respectively, to the case of multiple-structure rupture as:

$$C_1 = \frac{10^{b(M_{L1}-M_{L1+L2})} \times D_{L1+L2}}{D_{L1}} \tag{4}$$

and

$$C_2 = \frac{10^{b(M_{L2}-M_{L1+L2})} \times D_{L1+L2}}{D_{L2}}, \text{respectively} \tag{5}$$

where M_{L1} and M_{L2} represent the magnitudes of $L1$ and $L2$, respectively; D_{L1} and D_{L2} represent the displacements of $L1$ and $L2$, respectively; M_{L1+L2} represents the magnitude of the multiple-structure rupture; and D_{L1+L2} represents the displacement of the multiple-structure rupture.

The moment magnitude (M_w) of the multiple-structure rupture could be evaluated according to the rupture area (denoted as A) and fault types of the two seismogenic structures. In the TEM structure database, determination of rupture magnitude (Table 1) is based on the scaling law proposed by Wells and Coppersmith (1994), represented as:

Table 2 Potential pairs of multiple-structure ruptures, their parameters, and recurrence intervals of earthquakes

ID	Seismogenic structure name	Type	With minimum area		Recurrence interval (year)			With mean area		Recurrence interval (year)			With maximum area		Recurrence interval (year)		
			Area (km)	M_w	For min slip rate	For mean slip rate	For max slip rate	Area (km)	M_w	For min slip rate	For mean slip rate	For max slip rate	Area (km)	M_w	For min slip rate	For mean slip rate	For max slip rate
2, 3	Shuanglienpo structure, Yangmei structure	R, R	126.27	6.22	20,647	10,029	2489	208.14	6.42	27,419	13,281	3346	353.29	6.62	37,000	18,500	4604
2, 4	Shuanglienpo structure, Hukou fault	R, R	397.92	6.67	23,444	9953	2010	643.67	6.86	29,929	12,324	2499	1136.23	7.08	39,026	16,191	3287
4, 5	Hukou fault, Fengshan river strike-slip structure	R, LL	681.33	6.88	2141	1192	360	937.34	7	2794	1550	464	1390.65	7.16	4098	2254	668
4, 6	Hukou fault, Hsinchu fault	R, R	460.39	6.73	18,377	7574	1586	717.03	6.9	21,949	9250	1930	1201.64	7.1	28,556	11,953	2495
6, 8	Hsinchu fault, Hsinchu frontal structure	R, R	292.32	6.55	4000	1721	368	447.03	6.72	5096	2184	467	727.93	6.91	6809	2929	626
6, 9	Hsinchu fault, Touhuanping structure	R, RL	399.67	6.63	16,926	9723	2874	515.92	6.75	20,226	11,527	3268	670.22	6.86	24,140	13,120	3636
9, 10	Touhuanping structure, Miaoli frontal structure	RL, R	642.71	6.86	6423	2881	630	928.89	7	7204	3209	695	1451.16	7.18	8858	3914	842
10, 15	Miaoli frontal structure, Tuntzuchiao fault	R, RL	730.04	6.91	5510	2513	572	1018.95	7.04	6371	2870	643	1544.63	7.2	7811	3473	769
11, 14	Tunglo structure, Sanyi fault	R, R	671.08	6.87	11,664	4000	741	1146.05	7.08	15,090	5276	975	2094.44	7.32	21,747	7478	1387
13, 14	Shihtan fault, Sanyi fault	R, R	884.47	6.98	6920	2735	598	1379.38	7.16	9667	3757	806	2305.96	7.36	14,093	5391	1135
19, 22	Chiuchiungkeng fault, Muchiliao—Liuchia fault	R, R	933.6	7	998	539	151	1440	7.17	1270	691	196	2455.8	7.38	1755	965	278
20, 21	Meishan fault, Chiayi frontal structure	RL, R	1316.87	7.14	2104	1251	345	1952.58	7.29	2722	1553	409	3176.28	7.48	3871	2097	527

Table 2 (continued)

ID	Seismogenic structure name	Type	With minimum area		Recurrence interval (year)			With mean area		Recurrence interval (year)			With maximum area		Recurrence interval (year)		
			Area (km)	M_w	For min slip rate	For mean slip rate	For max slip rate	Area (km)	M_w	For min slip rate	For mean slip rate	For max slip rate	Area (km)	M_w	For min slip rate	For mean slip rate	For max slip rate
21, 41	Chiayi frontal structure, Tainan frontal structure	R, R	2073.57	7.32	4475	1966	438	3303.52	7.5	5726	2512	558	5713.1	7.71	7776	3402	755
22, 23	Muchiliao—Liuchia fault, Chungchou structure	R, R	865.13	6.97	364	271	184	1334.4	7.14	471	351	239	2275.71	7.35	663	494	337
24, 25	Hsinhua fault, Houchiali fault	RL, R	251.94	6.43	559	326	222	309.14	6.52	609	367	254	383.06	6.61	661	413	288
26, 45	Chishan fault, Fengshan structure	LL/R, LL/R	576	6.8	615	573	534	742.38	6.91	706	661	619	834.77	6.96	825	766	713
43, 45	Youchang sturcture, Fengshan structure	R/RL, LL/R	390.21	6.62	405	374	265	501.35	6.73	465	432	314	546.44	6.77	530	487	341

LL left-lateral strike-slip mechanism, *R* reverse mechanism, *RL* right-lateral strike-slip mechanism

Table 3 Multiple-structure rupture pairs considering different thresholds in structure distance and Coulomb stress change

ID	Seismogenic structure name	5.0 km				2.5 km				Max. distance between a pair
		0.01 bar	0.05 bar	0.1 bar	0.2 bar	0.01 bar	0.05 bar	0.1 bar	0.2 bar	ΔCFS triggering threshold
2, 3	Shuanglienpo structure, Yangmei structure	✓	✓	✓	✓	✓	✓	✓		
2, 4	Shuanglienpo structure, Hukou fault	✓	✓	✓	✓	✓	✓	✓	✓	
4, 5	Hukou fault, Fengshan river strike-slip structure	✓	✓	✓	✓	✓	✓	✓	✓	
4,6	Hukou fault, Hsinchu fault		✓	✓		✓	✓	✓		
4, 8	Hukou fault, Hsinchu frontal structure	✓	✓			✓				
6, 8	Hsinchu fault, Hsinchu frontal structure	✓	✓	✓	✓	✓	✓	✓	✓	
6, 9	Hsinchu fault, Touhuanping structure	✓	✓	✓	✓	✓				
9, 10	Touhuanping structure, Miaoli frontal structure	✓	✓	✓		✓	✓	✓		
10, 15	Miaoli frontal structure, Tuntzuchiao fault	✓	✓	✓	✓	✓	✓	✓	✓	
10, 16	Miaoli frontal structure, Changhua fault	✓	✓			✓	✓			
11, 14	Tunglo structure, Sanyi fault	✓	✓	✓		✓	✓	✓		
11, 16	Tunglo structure, Changhua fault	✓				✓				
13, 14	Shihtan fault, Sanyi fault	✓	✓	✓		✓	✓	✓		
13, 16	Shihtan fault, Changhua fault	✓				✓				
14, 17	Sanyi fault, Chelungpu fault	✓	✓			✓	✓			
15, 16	Tuntzuchiao fault,Changhua fault	✓				✓				
16, 19	Changhua fault, Chiuchiungkeng fault	✓	✓			✓	✓			
16, 20	Changhua fault, Meishan fault	✓				✓				
16, 40	Changhua fault, Gukeng structure	✓								
17, 19	Chelungpu fault, Chiuchiungkeng fault	✓				✓				
17, 20	Chelungpu fault, Meishan fault	✓				✓				
17, 40	Chelungpu fault, Gukeng structure	✓								
19, 22	Chiuchiungkeng fault, Muchiliao—Liuchia fault	✓	✓	✓	✓	✓				
20, 21	Meishan fault, Chiayi frontal structure	✓	✓	✓		✓	✓	✓		
21, 41	Chiayi frontal structure, Tainan frontal structure	✓	✓	✓		✓				
22, 23	Muchiliao—Liuchia fault, Chungchou structure	✓	✓	✓	✓	✓	✓	✓	✓	
23, 27	Chungchou structure, Hsiaokangshan fault	✓	✓			✓	✓			
24, 25	Hsinhua fault, Houchiali fault	✓	✓	✓		✓	✓	✓		
24, 41	Hsinhua fault, Tainan frontal structure	✓				✓				
26, 45	Chishan fault, Fengshan structure	✓	✓	✓	✓	✓		✓	✓	
27, 42	Hsiaokangshan fault, Longchuan structure	✓	✓			✓	✓			
30, 31	Hengchun fault, Hengchun offshore structure	✓								
32, 33	Milun fault, Longitudinal Valley fault	✓				✓				
43, 45	Youchang sturcture, Fengshan structure	✓	✓	✓	✓	✓				
	Total pairs of each criteria	34	23	17	10	31	18	13	6	

$$M_w = 4.33 + 0.90 \times log(A) \ldots \text{for reverse faulting;} \quad (6)$$

$$M_w = 3.98 + 1.02 \times log(A) \ldots \text{for strike} - \text{slip faulting;} \quad (7)$$

$$M_w = 3.93 + 1.02 \times log(A) \ldots \text{for normal faulting.} \quad (8)$$

We first follow the procedure of the TEM model to implement these scaling relations and then evaluate uncertainty of this procedure considering different scaling relations.

Based on the M_w–M_0 scale (Kanamori 1977) and the definition of seismic moment, average displacement of a seismogenic structure (D, in meters) could be evaluated according to M_w and A (in km^2):

$$D = \frac{10^{\frac{2}{3}M_w} \times 10^{-15.85}}{3A}. \quad (9)$$

The potential of multiple-structure ruptures could be attributed to the moment accumulation from the first and second structures, $L1$ and $L2$. We assumed their original slip rates, $\dot{D}_{L1}$ and $\dot{D}_{L2}$, could be partitioned into two cases, the rupture on the original structure and the rupture on multiple structures. The slip rate partitioned to individual structure ruptures ($L1$ and $L2$, respectively) can be represented as:

$$\dot{D}'_{L1} = \frac{\dot{D}_{L1}}{\left(\frac{A_{L1+L2}}{A_{L1}} \times C_1 + 1\right)} \text{ and} \quad (10)$$

$$\dot{D}'_{L2} = \frac{\dot{D}_{L2}}{\left(\frac{A_{L1+L2}}{A_{L2}} \times C_2 + 1\right)} \text{ respectively,} \quad (11)$$

where A_{L1} and A_{L2} represent the rupture areas of $L1$ and $L2$, respectively; A_{L1+L2} represents the area of the multiple-structure rupture. By integrating the obtained partitioned rates (Eqs. 10 and 11) and the slip rate partitioned to individual structure ruptures (Eqs. 4 and 5), the slip rate partitioned to the multiple-structure rupture from the original L1 and L2 can be obtained:

$$\dot{D}^{L1}_{L1+L2} = C_1 \times \dot{D}'_{L1} \text{ and} \quad (12)$$

$$\dot{D}^{L2}_{L1+L2} = C_2 \times \dot{D}'_{L2}, \text{respectively.} \quad (13)$$

Then the sum of the slip rates for the multiple-structure rupture is calculated using the partitioned rates of the two structures, represented as:

$$\dot{D}_{L1+L2} = \dot{D}^{L1}_{L1+L2} + \dot{D}^{L2}_{L1+L2}. \quad (14)$$

Following the assumption presented in Eq. 2, considering the displacement and slip rate, recurrence intervals for individual structures (R_{L1} and R_{L2}) and the multiple-structure rupture (R_{L1+L2}) can be represented as:

$$R_{L1} = \frac{D_{L1}}{\dot{D}'_{L1}}, \quad (15)$$

$$R_{L2} = \frac{D_{L2}}{\dot{D}'_{L2}}, \text{and} \quad (16)$$

$$R_{L1+L2} = \frac{D_{L1+L2}}{\dot{D}_{L1+L2}}, \text{respectively.} \quad (17)$$

3.2 Single structure contributes to several multiple-structure ruptures

A single seismogenic structure could be involved in multiple cases of multiple-structure rupture. For such cases, however, evaluation of the corresponding recurrence intervals has seldom been discussed. Here, we propose a procedure for quantifying the return period of this case, shown below.

When a single structure ($L1$) is involved in multiple cases of multiple-structure rupture ($L1+L2$, …, $L1+Ln$), the slip rate partitioned to the original structure can be obtained based on the revision of Eq. 10, represented as:

$$\dot{D}'_{L1} = \frac{A_{L1} \times \dot{D}_{L1} \times D_{L1}}{(A_{L1} \times D_{L1}) + \sum_{i=2}^{n}\left(A_{L1+Li} \times D_{L1+Li} \times 10^{b(M_{L1}-M_{L1+Li})}\right) + \sum_{i=2}^{n-1}\sum_{j=3}^{n}\left(A_{L1+Li+Lj} \times D_{L1+Li+Lj} \times 10^{b(M_{L1}-M_{L1+Li+Lj})}\right) + \sum_{i=2}^{n-2}\sum_{j=3}^{n-1}\sum_{k=4}^{n}\cdots}, \quad 1 < \mathrm{i} < \mathrm{j} < \mathrm{k}. \quad (18)$$

where D_{L1+L2}, ….,D_{L1+Ln} represent the displacements of the multiple-structure rupture cases $L1+L2$, …, $L1+L$n, respectively.

The slip rate partitioned to the multiple-structure rupture cases $L1+L2$, …, $L1+L$n can be represented as:

$$\dot{D}^{L1}_{Lx} = \frac{A_{L1} \times \dot{D}_{L1} \times D_{L1+Lx} \times 10^{b(M_{L1}-M_{Lx})}}{(A_{L1} \times D_{L1}) + \sum_{i=2}^{n}(A_{L1+Li} \times D_{L1+Li} \times 10^{b(M_{L1}-M_{L1+Li})}) + \sum_{i=2}^{n-1}\sum_{j=3}^{n}(A_{L1+Li+Lj} \times D_{L1+Li+Lj} \times 10^{b(M_{L1}-M_{L1+Li+Lj})}) + \sum_{i=2}^{n-2}\sum_{j=3}^{n-1}\sum_{k=4}^{n}\cdots}, \quad Lx = L1+Li+Lj+Lk+\ldots \quad (19)$$

respectively. In this case, evaluation of the recurrence interval for each multiple-structure rupture requires the slip rates contributed from two structures as well, similar to what is shown in Eq. 14. The total slip rate for each case of multiple-structure rupture can be represented as:

$$\dot{D}_{Lx} = \dot{D}^{L1}_{Lx} + \sum_{i=2}^{n}\dot{D}^{Li}_{Lx}. \quad (20)$$

The recurrence intervals for each multiple-structure rupture case can be represented as:

$$R_{Lx} = \frac{D_{Lx}}{\dot{D}_{Lx}}, \tag{21}$$

while the recurrence intervals for the original structure is represented in Eq. 15.

A single earthquake could be attributed to multiple (more than three) structures, for example, the 2010 El Mayor-Cucapah, US, earthquake (Wei et al. 2011); the 2016 M_w7.8 Kaikōura, New Zealand, earthquake (Hamling et al. 2017). In such special cases, the recurrence interval can be also evaluated through the procedure mentioned above. Thus, rupture probability of multiple structures could be quantified, which could constrain subsequent probabilistic seismic hazard assessment.

3.3 Multiple-structure rupture recurrence intervals and uncertainties

According to the structure parameters, the recurrence intervals of each pair of potential multiple-structure ruptures can be evaluated. Considering the 17 pairs with $\Delta CFS \geq 0.1$ bar and distance ≤ 5.0 km (listed in Table 2),

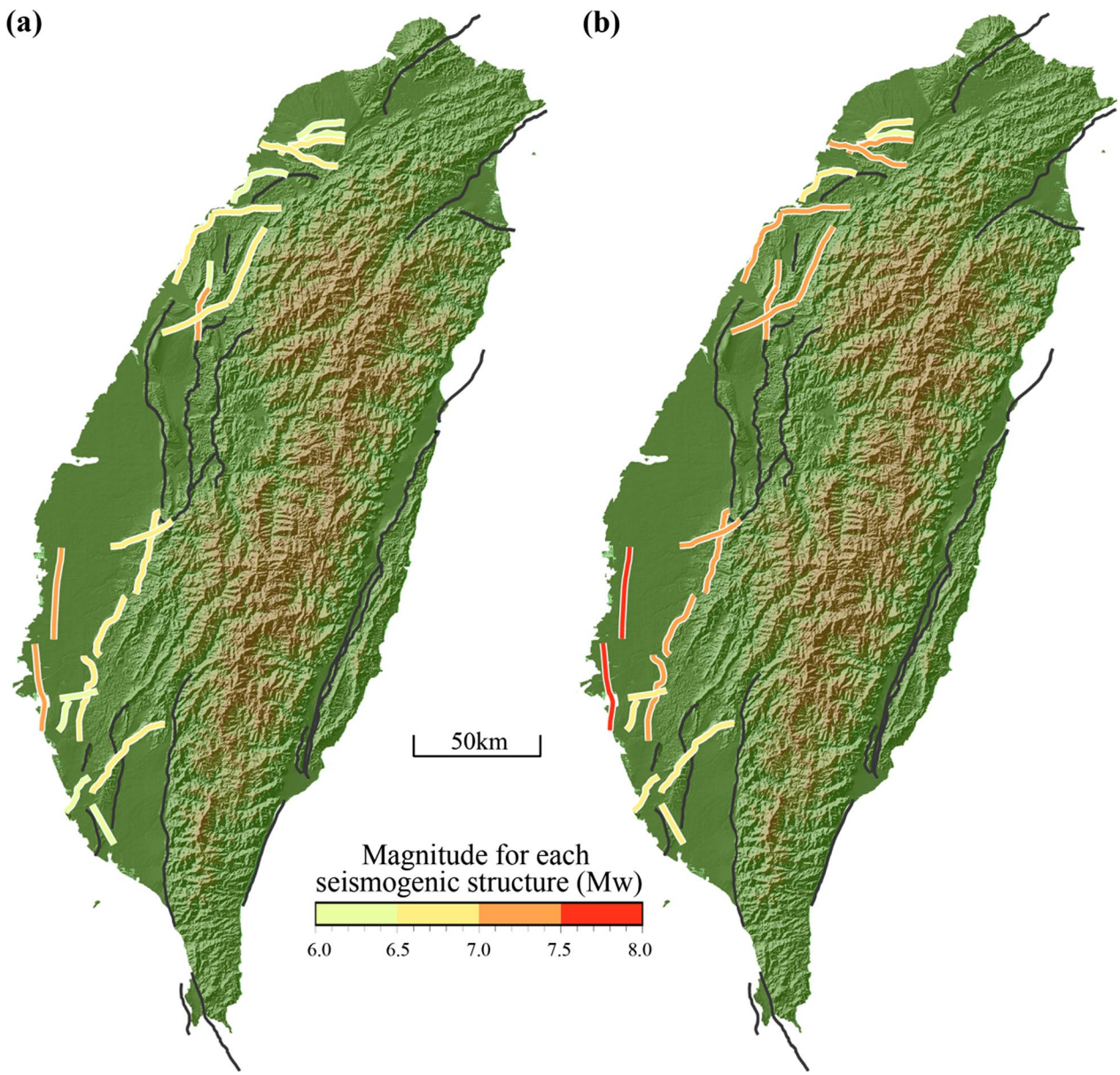

Fig. 3 Magnitudes for the seismogenic structures (**a**) by the TEM database and (**b**) considering multiple structure rupture pairs with $\Delta CFS \geq 0.1$ bar and distance ≤ 5.0 km. Corresponding parameters for the structures and multiple-structure ruptures are listed in Tables 1 and 2

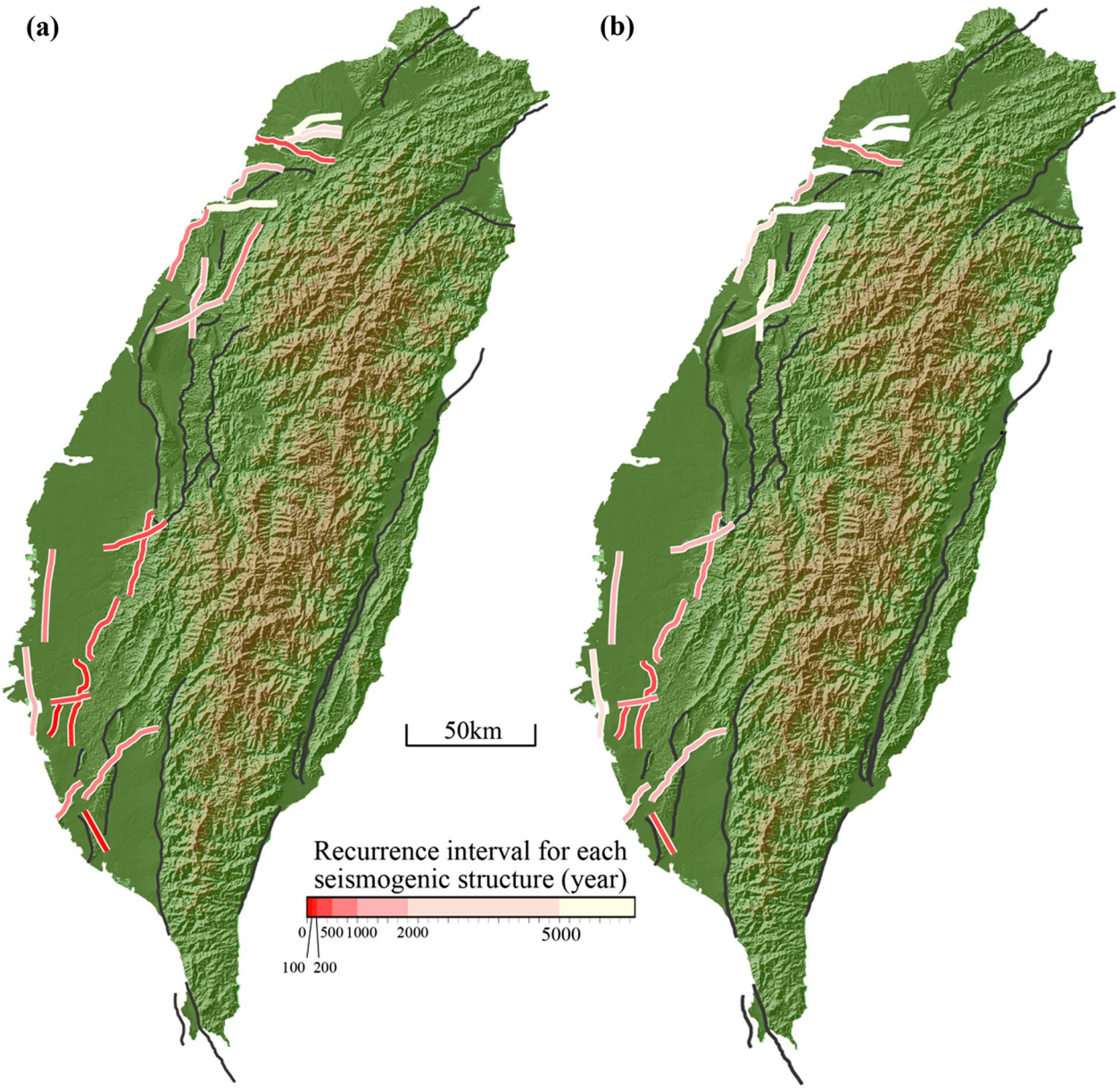

Fig. 4 Recurrence interval for the seismogenic structures (**a**) by the TEM database and (**b**) considering multiple structure rupture pairs with ΔCFS ≥ 0.1 bar and distance ≤ 5.0 km. Corresponding parameters for the structures and multiple-structure ruptures are listed in Tables 1 and 2

we evaluated their potential magnitudes (Fig. 3) and recurrence intervals (Fig. 4). In addition to the mean value of each parameter, we quantified epistemic uncertainties from deviations of slip rate and rupture area. The largest magnitude is expected if the maximum rupture areas of the two structures are assumed (based on Eqs. 6–8). Also, the shortest recurrence interval is expected if the minimum rupture area and maximum slip rate are assumed (based on Eqs. 4–17).

In comparison with the original recurrence intervals of the structures without considering a multiple-structure rupture (Table 4), longer recurrence intervals are expected for multiple-structure ruptures and individual structures due to slip partitioning.

Additionally, our results show that a single seismogenic structure sometimes pairs with several cases of multiple-structure ruptures. For example, the Hukou fault (ID 4) potentially ruptures with the Shuanglianpo structure (ID

Table 4 Original and revised recurrence intervals of the seismogenic structures that involve the cases of multiple-structure rupture

ID	Seismogenic structure name	Type	Original slip rate (mm/year)	Multiple slip rate (mm/year)	Original recurrence interval (year)	Multiple recurrence interval (year)
2	Shuanglienpo structure	R	0.13	0.033	5540	21,818
3	Yangmei structure	R	0.18	0.074	3330	8106
4	Hukou fault	R	0.46	0.104	2520	11,154
5	Fengshan river strike-slip structure	SS	3.18	1.337	300	710
6	Hsinchu fault	R	0.66	0.125	1260	6640
8	Hsinchu frontal structure	R	1.44	0.642	1170	1401
9	Touhuanping structure	SS	0.13	0.034	6150	23,529
10	Miaoli frontal structure	R	1.84	0.547	660	2230
11	Tunglo structure	R	0.5	0.151	1360	4509
13	Shihtan fault	R	1.38	0.519	720	1908
14	Sanyi fault	R	0.85	0.269	1710	5390
15	Tuntzuchiao fault	SS	0.5	0.204	1880	4601
19	Chiuchiungkeng fault	R	4.66	2.093	290	503
20	Meishan fault	SS	2.51	0.871	350	1059
21	Chiayi frontal structure	R	3.36	0.992	510	1724
22	Muchiliao—Liuchia fault	R	5.75	1.573	210	782
23	Chungchou structure	R	12.2	5.393	100	237
24	Hsinhua fault	SS	2.65	1.238	260	557
25	Houchiali fault	R	7.07	2.806	90	217
26	Chishan fault	SS/R	1.1	0.492	880	1971
41	Tainan frontal structure	R	0.92	0.405	1890	4294
43	Youchang sturcture	R/SS	1.64	0.699	510	1188
45	Fengshan structure	SS/R	10	2.604	75	288

LL left-lateral strike-slip mechanism, *N* normal mechanism, *R* reverse mechanism, *RL* right-lateral strike-slip mechanism

2), the Fengshan river strike-slip structure (ID 5), and the Hsinchu fault (ID 6), while the Hsinchu fault (ID 6) could also result in multiple-segment ruptures with the Hsinchu frontal structure (ID 8) and the Touhuanping structure (ID 9). Besides these two cases associated with three rupture pairs, several structures could be associated with two multiple-structure pairs (Table 2), raising the importance of implementing slip partitioning from a single structure to several multiple-structure ruptures. Based on our analysis, it might be difficult for the structures that pair with several cases of multiple-structure ruptures might to rupture solely. That is, based on Eqs. 18–22, the slip rate of these structures could be partitioned to several cases of multiple-structure ruptures, resulting in longer recurrence intervals. For example, the Hukou fault (ID 4) and the Hsinchu fault (ID 6) involved four and three pairs of multiple-structure ruptures, respectively (Table 2), and their recurrence intervals became 4.4 and 5.3 times, respectively, longer than the cases without considering multiple-structure ruptures (Table 4).

Our calculations of recurrence interval for the multiple-structure ruptures are based on the scaling relations proposed by Wells and Coppersmith (1994). These relationships were obtained based on the global data summarized decades ago. To validate the sensitivity of our procedure to scaling, here we implement alternative scaling law proposed by Yen and Ma (2011), who investigated the rupture parameters of the earthquakes mainly from the Taiwan orogenic belt. This relation illustrates average displacement of a seismogenic structure (D, in meters) as a constant:

$$Log(D) = -0.32. \tag{22}$$

Based on this relation, recurrence intervals for each multiple-structure rupture pairs were evaluated (Table 5). Comparing these to those obtained by Wells and Coppersmith's relations, shorter recurrence intervals were obtained (Fig. 4 and Table 2), especially for those with larger magnitude (Fig. 3 and Table 2). These results can be attributed to a smaller average displacement obtained for a large event that led to a shorter recurrence interval for the multiple-structure rupture (based on Eq. 17).

Table 5 Potential pairs of multiple-structure ruptures, their parameters, recurrence intervals of earthquakes evaluated by the scaling laws of Wells and Coppersmith (1994) and Yen and Ma (2011), respectively, and their differences

ID	Seismogenic structure name	Type	Area (km^2)	M_w	Recurrence interval (year)		Difference, %
					W&C*	Y&M#	
2, 3	Shuanglienpo structure, Yangmei structure	R, R	208.1	6.42	13,281	8863	− 33.3
2, 4	Shuanglienpo structure, Hukou fault	R, R	643.7	6.86	12,324	6381	− 48.2
4, 5	Hukou fault, Fengshan river strike-slip structure	R, LL	937.3	7.00	1550	950	− 38.7
4, 6	Hukou fault, Hsinchu fault	R, R	717.0	6.90	9250	4739	− 48.8
6, 8	Hsinchu fault, Hsinchu frontal structure	R, R	447.0	6.72	2184	1429	− 34.6
6, 9	Hsinchu fault, Touhuanping structure	R, RL	515.9	6.75	11,527	6058	− 47.4
9, 10	Touhuanping structure, Miaoli frontal structure	RL, R	928.9	7.00	3209	1703	− 46.9
10, 15	Miaoli frontal structure, Tuntzuchiao fault	R, RL	1019.0	7.04	2870	1564	− 45.5
11, 14	Tunglo structure, Sanyi fault	R, R	1146.1	7.08	5276	2766	− 47.6
13, 14	Shihtan fault, Sanyi fault	R, R	1379.4	7.16	3757	2019	− 46.3
19, 22	Chiuchiungkeng fault, Muchiliao—Liuchia fault	R, R	1440.0	7.17	691	385	− 44.3
20, 21	Meishan fault, Chiayi frontal structure	RL, R	1952.6	7.29	1553	743	− 52.2
21, 41	Chiayi frontal structure, Tainan frontal structure	R, R	3303.5	7.50	2512	1224	− 51.3
22, 23	Muchiliao—Liuchia fault, Chungchou structure	R, R	1334.4	7.14	351	202	− 42.5
24, 25	Hsinhua fault, Houchiali fault	RL, R	309.1	6.52	367	281	− 23.4
26, 45	Chishan fault, Fengshan structure	LL/R, LL/R	742.4	6.91	661	383	− 42.1
43, 45	Youchang sturcture, Fengshan structure	R/RL, LL/R	501.4	6.73	432	252	− 41.7

*W&C: The scaling law by Wells and Coppersmith (1994)

Y&M: The scaling law by Yen and Ma (2011)

4 Discussion and conclusion

4.1 Interaction between structures and possible coseismic ruptures

In this study, we explored possible coseismic multiple-structure ruptures and quantified their recurrence intervals by implementing the Coulomb stress change and the Gutenberg-Richter law, respectively. The analyzing procedure we proposed is based on physics- and statistics-based models, and the outcomes are reproducible.

We compared our results with Shyu et al.'s (2020) conclusion that some seismogenic structure pairs—such as the Hsinchu fault (ID 6) and the Hsinchu frontal structure (ID 8), the Touhuanping fault (ID 9) and the Miaoli frontal structure (ID 10), the Meishan fault (ID 20) and the Chiayi frontal structure (ID 21), and the Chiayi frontal structure (ID 21) and the Tainan frontal structure (ID 41)—could rupture simultaneously. Their findings were consistent with our results based on the Coulomb stress triggering, as long as they defined seismogenic structure pairs according to geological and geomorphological evidence instead.

Additionally, Shyu et al. (2020) suggested some other structure pairs for multiple-structure ruptures, such as the Shihtan fault (ID 13) and Tuntzuchiao fault (ID 15), the Houchiali fault (ID 25) and the Tainan frontal structure (ID 41), and the Chaochou fault (ID 29) and the Hengchun fault (ID 30). These pairs, however, do not fit our hypothesis. Take the Shihtan and Tuntzuchiao faults, for example. The rupture of the Tuntzuchiao fault could result in a Coulomb stress increase of more than 0.1 bar in 79% of the sub-faults of the Shihtan fault, whereas only 2% of the sub-fault in the Tuntzuchiao fault would be triggered when the Shihtan fault dislocates (Additional file 1: Table S1). Note that the 1935 Hsinchu-Taichung earthquake is attributed to a coseismic rupture on the two faults. Previous studies (Yen et al. 2016; Su 2019) indicated that this earthquake did not initiate on either the Shihtan or the Tuntzuchiao fault, but on a blind fault linking the two. Since the database we accessed (Shyu et al. 2020) did not include this blind structure, our analysis could be further improved through better understanding seismogenic structures. In addition, we discussed the interaction between structures through a kinematic model; it is desired to further incorporate dynamic models (e.g., Brodsky and van der Elst 2014; Jiao et al. 2022; Lin 2021; Ulrich et al. 2016) to constrain the behaviors of multiple-structure ruptures.

In 1906, an earthquake with magnitude 7.1 occurred due to the rupture of the Meishan fault (ID 20). Considering its fault geometry, the characteristic magnitude of this fault is only 6.6 (Table 1); therefore, this event with a larger magnitude could be associated with a

multiple-structure rupture. In addition, the focal mechanism of this earthquake suggests that this event cannot be attributed solely to the rupture on the Meishan fault. The first motions of P- and S-waves recorded by the seismograph suggest oblique thrust faulting oriented in the northeast-southwest direction, with a small right-lateral component (Liao et al. 2018). Besides, large ground shaking with liquefaction took place to the west of the Meishan fault during the coseismic period (Omori 1906). According to the evidence mentioned above, the Chiayi frontal structure might rupture simultaneously. Considering parameters of the Meishan fault and the Chiayi frontal thrust (structure geometry, characteristic slip), when the Meishan fault is dislocated, the Coulomb stress on 64% of the Chiayi frontal structure plane may rise by more than 0.1 bar, and when the Chiayi frontal structure is dislocated, 72% of the Meishan fault could be closer to failure (Additional file 1: Table S1). In addition, the distance between the two faults is 1.87 km (Additional file 2: Table S2). Therefore, we concluded that these two structures could have mutually ruptured in a coseismic period and resulted in an event with magnitude 7.1 in 1906.

4.2 Uncertainty of multiple-structure rupture pair identification

In this study, we identified potential rupture pairs by considering Coulomb stress change along the shear and normal components and the effective friction coefficient (Eq. 1). We simplified this model without implementing a poroelastic assumption (Beeler et al. 2000), since previous studies (e.g., Chan and Stain 2009) concluded that the differences in their results were trivial for assuming reasonable values of Skempton's coefficients (between 0.5 and 0.9) and dry friction (0.75). The effective friction coefficient (μ') could alter the impact of normal stress change on the Coulomb stress change (ΔCFS). Since effective friction coefficients vary for different tectonic regimes, to quantify the deviation on determining multiple-rupture pairs, we further considered $\mu' = 0.2$ and 0.5. Considering the stress threshold of $\Delta CFS \geq 0.1$ bar and distance threshold of 5 km, the potential paired structures were identified (Table 6). The results suggest slight differences in the reasonable effective friction coefficient in between 0.2 and 0.5.

Table 6 Multiple-structure rupture pairs considering different effective friction coefficients (μ')

μ'	0.2	0.4	0.5	
Paired structures at each specific rake condition	2 3	2 3	*2 3*	2 3 Paired structures at the condition 2 3 Not paired structures at the condition
	2 4	2 4	2 4	
	4 5	4 5	4 5	
	4 6	4 6	4 6	
	6 8	6 8	6 8	
	6 9	6 9	6 9	
	9 10	9 10	9 10	
	10 15	10 15	*10 15*	
	11 14	11 14	11 14	
	13 14	13 14	13 14	
	16 18	*16 18*	16 18	
	19 22	19 22	19 22	
	20 21	20 21	20 21	
	21 41	21 41	21 41	
	22 23	22 23	22 23	
	24 25	24 25	24 25	
	26 28	*26 28*	26 45	
	26 45	26 45	43 45	
	27 42	*27 42*	*27 42*	
	43 45	43 45	43 45	
Number of pair	18	17	17	

In this study, we identified potential rupture pairs by considering thresholds of stress change and structure distance. We implemented four threshold sets of Coulomb stress change ($+0.01, +0.05, +0.1$, and $+0.2$ bars) and two for distance between structures (2.5 and 5.0 km) to identify plausible pairs for multiple-structure rupture (Table 3). Also, the uncertainty of the structure rake angle could result in deviation. Our standard procedure assumed a fixed rake angle of each structure according to its rupture type (Table 1), while in reality its rupture orientation could alter slightly in small patches of the structure plane.

We expected a long distance between two structures could make it difficult for the two structures to rupture simultaneously. Thus, we followed the criterion by the UCERF3 (Field et al. 2014) and SHERIFS (Chartier et al. 2017) and assumed a distance threshold of 5 km. We are aware that an earthquake with a large coseismic slip dislocation could result in significant stress change in far field and then search the pairs with longer distances and significant stress increase. Two additional distance thresholds of 10 and 20 km were considered (Table 7), and 6 and 9 additional pairs that might rupture in a coseismic period were identified, respectively. Generally, potential magnitudes of these structures are relatively large, which could result in larger stress perturbation. For example, the Chiayi frontal structure could cause an event with magnitude 7.21, resulting in a Coulomb stress increase of more than 0.1 bar in 91% of the sub-faults of the Chungchou structures, when 80% of the sub-fault in the Chiayi frontal structure would be triggered when the Chungchou structures dislocates with an M6.89 event (Additional file 1: Table S1).

To evaluate the impact of rake angle orientation, we evaluated the Coulomb stress change on the receiving structure with different rotated rake angles (i.e., $\pm 10°$ and $\pm 20°$). The results showed that the larger the rotated

Table 7 Multiple-structure rupture pairs considering different thresholds in structure distance

ID	Seismogenic structure name	20.0 km	10.0 km	5.0 km	2.5 km	Max. distance between a pair
2, 3	Shuanglienpo structure, Yangmei structure	✓	✓	✓	✓	
2, 4	Shuanglienpo structure, Hukou fault	✓	✓	✓	✓	
4, 5	Hukou fault, Fengshan river strike-slip structure	✓	✓	✓	✓	
4,6	Hukou fault, Hsinchu fault	✓	✓	✓	✓	
5, 7	Fengshan river strike-slip structure, Hsincheng fault	✓	✓			
6, 8	Hsinchu fault, Hsinchu frontal structure	✓	✓	✓	✓	
6, 9	Hsinchu fault, Touhuanping structure	✓	✓	✓		
7,10	Hsincheng fault, Miaoli frontal structure	✓	✓			
8, 12	Hsinchu frontal structure, East Miaoli structure	✓	✓			
9, 10	Touhuanping structure, Miaoli frontal structure	✓	✓	✓	✓	
10, 15	Miaoli frontal structure, Tuntzuchiao fault	✓	✓	✓	✓	
10, 16	Miaoli frontal structure, Changhua fault					
11, 14	Tunglo structure, Sanyi fault	✓	✓	✓	✓	
11, 16	Tunglo structure, Changhua fault					
12, 15	East Miaoli structure, Tuntzuchiao fault	✓				
13, 14	Shihtan fault, Sanyi fault	✓	✓	✓	✓	
19, 22	Chiuchiungkeng fault, Muchiliao—Liuchia fault	✓	✓	✓		
20, 21	Meishan fault, Chiayi frontal structure	✓	✓	✓	✓	
21, 23	Chiayi frontal structure, Chungchou structure	✓	✓			
21, 41	Chiayi frontal structure, Tainan frontal structure	✓	✓	✓		
22, 23	Muchiliao—Liuchia fault, Chungchou structure	✓	✓	✓	✓	
23, 44	Chungchou structure, Fengshan hills frontal structure	✓				
24, 25	Hsinhua fault, Houchiali fault	✓	✓	✓	✓	
26, 45	Chishan fault, Fengshan structure	✓	✓	✓	✓	
27, 44	Hsiaokangshan fault, Fengshan hills frontal structure	✓	✓			
28, 43	Kaoping River structure, Youchang sturcture	✓	✓			
39, 40	Chushiang structure, Gukeng structure	✓				
43, 45	Youchang sturcture, Fengshan structure	✓	✓	✓		
	Total pairs of each criteria	26	23	17	13	

rake angles implemented for the receiver structures, the fewer structure pairs were identified (Table 8). Note that 11 pairs were identified even when the rakes rotated for $\pm 20°$, suggesting their robustness for coseismic multiple-structure rupture.

4.3 Uncertainty of recurrence interval

Besides the uncertainty of structure pair identification, uncertainties in the rupture parameters of the multiple structures could be evaluated. Considering the range of the structures' rupture areas (Table 1), magnitude intervals of multiple-structure ruptures could be estimated (Fig. 4 and Table 2). That is that the largest magnitude for multiple-structure rupture (Fig. 3) can be obtained when we consider the maximum rupture areas of the two structures (based on Eqs. 6–8). By further implementing structure slip rates, recurrence intervals can be quantified: the minimum rupture area and maximum slip rate obtains the shortest recurrence interval (based on Eqs. 4–17).

Rupture recurrence intervals could also be influenced by the implemented scaling relations. We proposed two relations, that is, in addition to the well-known relations by Wells and Coppersmith (1994), we also used the relations proposed by Yen and Ma (2011) that were obtained from the observations mainly from Taiwan. Since the local relationships (Yen and Ma 2011) infer a smaller displacement, shorter recurrence intervals were obtained (Table 5). Besides, although the scaling relations proposed by Wells and Coppersmith (1994) have been questioned by many modern models, especially for large megathrusts (e.g., Stirling et al. 2013), Wang et al. (2016b) concluded a similar maximal magnitude of each seismogenic structure estimated from the relations of Wells and Coppersmith (1994) and Yen and Ma (2011).

Table 8 Potential paired structures considering various rake angle rotations. In these cases, the stress threshold of ΔCFS ≥ 0.1 bar and distance threshold of 5 km were considered to identify potential rupture pairs. The total number of paired structures without rake rotation is 17 (Table 2)

Rake angle rotation	+ 10°	− 10°	+ 20°	− 20°	
Paired structures at each specific rake condition	2 3	2 3	2 3	2 3	2 3 Paired structures at the condition 2 3 Not paired structures at the condition
	2 4	2 4	*2 4*	2 4	
	4 5	4 5	4 5	*4 5*	
	4 6	4 6	4 6	*4 6*	
	6 8	6 8	6 8	6 8	
	6 9	6 9	*6 9*	6 9	
	9 10	9 10	9 10	*9 10*	
	10 15	10 15	10 15	10 15	
	11 14	11 14	*11 14*	*11 14*	
	13 14	13 14	*13 14*	13 14	
	19 22	19 22	19 22	19 22	
	20 21	20 21	20 21	20 21	
	21 41	21 41	21 41	21 41	
	22 23	22 23	22 23	22 23	
	24 25	*24 25*	24 25	*24 25*	
	26 45	26 45	26 45	26 45	
	43 45	*43 45*	43 45	*43 45*	
Number of pair	16	15	13	11	
Number of pairs without rake angle rotation: 17					

In these cases, the stress threshold of ΔCFS ≥ 0.1 bar and distance threshold of 5 km were considered to identify potential rupture pairs. The total number of paired structures without rake rotation is 17 (Table 2)

For recurrence interval, the magnitude-frequency distribution on a single-structure plays an important role. Evaluating the rupture recurrence interval on a single structure could be based on various models, for example, the Gutenberg-Richter law (Gutenberg and Richter 1944), the characteristic earthquake model (Youngs and Coppersmith 1985; Hecker et al. 2013; Stirling and Zungia 2017) in addition to others (e.g., Geist and Parsons 2019; Page et al. 2021). In this study, we evaluated the rupture recurrence interval as the ratio of slip of a characteristic earthquake (with maximum magnitude of the structure) and slip rate, shown as Eq. 2, based on the assumption proposed by the TEM seismogenic structure database (Shyu et al. 2020) and the TEM PSHA2020 (Chan et al. 2020). This factor could be replaced by other magnitude-frequency distributions since the recurrence interval of the multiple-structure rupture in our procedure is based on slip rate partitioned from individual structure ruptures (shown as Eqs. 10, 11, 14, 18, and 20).

Based on our analyses mentioned above, deviations of multiple-structure rupture pairs were indicated, and epistemic uncertainties of corresponding parameters were quantified, providing a better understanding of multiple-structure rupture behaviors, beneficial to subsequent research, such as PSHA, mentioned below.

4.4 Application of multiple-structure rupture to probabilistic seismic hazard analysis

Conducting a PSHA requires understanding potential magnitude (Fig. 3) and the recurrence interval (Fig. 4) of each seismogenic source, and implementing a hazard model with multiple-structure rupture could improve the assessment. Take the TEM PSHA2020 (Chan et al. 2020) as an example—considering the cases of multiple-structure ruptures, the hazard levels in the regions close to the Chaochou fault (ID 29) and the Tainan frontal structure (ID 41) increased significantly for a long return period (recurrence interval of 2475 years, see Fig. 3 of Chan et al. 2020). Chan et al.'s study (2020) indicated that the seismic hazard level would be misestimated if the probability of multiple-structure rupture is not implemented.

Seismic hazard analysis plays an essential role in constructing infrastructures, such as nuclear power plants, that require assuming a long return period. Thus, a seismogenic source with a long recurrence interval could be crucial for the analysis, raising the importance of multiple-fault rupture with a larger magnitude (larger than the characteristic earthquake of each structure). Our

approach obtained longer recurrence intervals for multiple-structure ruptures in comparison with the original recurrence interval of each structure (Table 4). For example, the recurrence interval of the Chiayi frontal structure (ID 21) has been extended from 510 to 1724 years. Based on these results, the seismic hazard level for a short return period (e.g., 475 years, corresponding to a 10% probability exceedance in 50 years) would be lower, while a higher hazard is expected for a long return period (e.g., 2475 years, corresponding to a 2% probability exceedance in 50 years).

The possibility of multiple-structure rupture used to be determined based on geological and geomorphological evidence with subjective judgments (e.g., Shyu et al. 2020). Our study implemented a Coulomb stress change combined with statistical approaches to indicate multiple-structure rupture pairs, which is transparent and reproducible.

In addition, our approach indicated various rupture pairs and quantified uncertainties. These outcomes could be incorporated into a PSHA through a logic tree. For example, larger weightings (possibilities) could be assumed for the pairs that fulfill more thresholds in the distance, Coulomb stress change (Table 3) and rotated rake angles (Table 8). That includes, for instance, the Shuanglianpo fault (ID 2) and the Hukou fault (ID 4); the Hukou fault (ID 4) and the Fengshan River strike-slip structure (ID 5); the Hsinchu fault (ID 6) and the Hsinchu frontal structure (ID 8); the Miaoli frontal structure (ID 10) and Tuntzuchiao fault (ID 15); the Muchiliao-Liuchia fault (ID 22) and the Chungchou structure (ID 23); and the Chishan fault (ID 26) and the Fengshan structure (ID 45).

4.5 Multiple structure rupture (with more than three structures)

The 2016 M_w7.8 Kaikōura, New Zealand, earthquake is an event resulting from ruptures on multiple structures. Hamling et al. (2017) indicated that this earthquake included ruptures along four major faults and up to twelve minor faults. From this case, we are aware that multiple-structure rupture is not limited to the combination of two seismogenic structures.

Based on the multiple-structure rupture database proposed in this study (Table 2), several structures are associated with several possible rupture pairs. For instance, the Shuanglianpo fault (ID 2) may cause coseismic rupture with the Yangmei structure (ID 3) and the Hukou fault (ID 4), and the Hukou fault (ID 4) may link with the Fengshan River strike-slip structure (ID 5) and the Hsinchu fault (ID 6). Since our approach is based on a static Coulomb stress change, it is difficult to evaluate the temporal evolution of rupture probability. The possibility of a multiple-structure rupture in a coseismic period might be overestimated, that is, a structure could not only be triggered spontaneously in a coseismic period, but also be enhanced in a postseismic or interseismic period.

One potential solution is to implement a dynamic model (e.g., a discrete element model; Cundall and Strack 1979) that simulates temporal distribution of displacement and stress fields and could be helpful in identifying plausible structures that perhaps rupture within a coseismic period.

Supplementary Information

The online version contains supplementary material available at https://doi.org/10.1007/s44195-023-00040-8.

Additional file 1. Table S1: The ratio of triggering between each pair of structural planes. Note that the same pair may have a different ratio when the source and receiver structures are switched.

Additional file 2. Table S2: The distance between each pair of structures.

Acknowledgements

This study was supported by the Ministry of Science and Technology in Taiwan under the grants MOST 109-2116-M-008 -029 -MY3, MOST 110-2124-M-002 -008, and MOST 110-2634-F-008-008. This work is financially supported by the Earthquake-Disaster & Risk Evaluation and Management Center (E-DREaM) from the Featured Areas Research Center Program within the framework of the Higher Education Sprout Project by the Ministry of Education in Taiwan. The authors thank the editor, Frédéric Deschamps, and two anonymous reviewers for their constructive comments.

Author contributions

CCC and CYU performed the analyses and conducted the numerical modeling. JCG replied reviewers' comments. CHC developed the methodologies and administrated the project. All authors contributed to scientific discussion, critical validation of results, and writing the manuscript. All authors read and approved the final manuscript.

Declarations

Competing interests

The authors declare that they have no conflict of interest.

Received: 17 October 2022 Accepted: 11 April 2023
Published online: 25 May 2023

References

Beeler N, Simpson R, Hickman S, Lockner D (2000) Pore fluid pressure, apparent friction, and Coulomb failure. J Geophys Res 105(25):533–625
Brodsky EE, van der Elst NJ (2014) The uses of dynamic earthquake triggering. Annu Rev Earth Planet Sci 42:317–339
Catalli F, Chan CH (2012) New insights into the application of the Coulomb model in real-time. Geophys J Int 188(2):583–599
Chan CH, Stein RS (2009) Stress evolution following the 1999 Chi-Chi, Taiwan, earthquake: consequences for afterslip, relaxation, aftershocks and departures from Omori decay. Geophys J Int 177(1):179–192
Chan CH, Ma KF, Shyu JBH, Lee YT, Wang YJ, Gao JC et al (2020) Probabilistic seismic hazard assessment for Taiwan: TEM PSHA2020. Earthq Spectra 36(1_suppl):137–159

Chartier T, Scotti O, Lyon-Caen H, Boiselet A (2017) Methodology for earthquake rupture rate estimates of fault networks: example for the western Corinth rift, Greece. Nat Hazard 17(10):1857–1869
Chartier T, Scotti O, Lyon-Caen H (2019) SHERIFS: Open-source code for computing earthquake rates in faultsystems and constructing hazard models. Seismol Res Lett 90(4):1678–1688
Cundall PA, Strack ODL (1979) Discrete numerical model for granular assemblies. Geotechnique 29:47–65
Field EH, Arrowsmith RJ, Biasi GP, Bird P, Dawson TE, Felzer KR et al (2014) Uniform California earthquake rupture forecast, version 3 (UCERF3)—the time-independent model. Bull Seismol Soc Am 104(3):1122–1180
Geist EL, Parsons T (2019) A combinatorial approach to determine earthquake magnitude distributions on a variable slip-rate fault. Geophys J Int 219(2):734–752
Gutenberg B, Richter CF (1944) Frequency of earthquakes in California. Bull Seismol Soc Am 34(4):185–188
Hamling IJ, Hreinsdóttir S, Clark K, Elliott J, Liang C, Fielding E et al (2017) Complex multifault rupture during the 2016 M w 7.8 Kaikōura earthquake, New Zealand. Science 356(6334):eaam7194
Hecker S, Abrahamson NA, Wooddell KE (2013) Variability of displacement at a point: implications for earthquake-size distribution and rupture hazard on faults. Bull Seismol Soc Am 103(2A):651–674
Jiao L, Chan CH, Scholtès L, Hubert-Ferrari A, Donzé FV, Tapponnier P (2022) Discrete element modeling of a subduction zone with a seafloor irregularity and its impact on the seismic cycle. Acta Geol Sin. https://doi.org/10.1111/1755-6724.14935
King GCP, Stein RS, Lin J (1994) Static stress changes and the triggering of earthquakes. Bull Seismol Soc Am 84:935–953
Liao Y, Ma K, Hsieh M, Cheng S, Kuo-Chen H, Chang C (2018) Resolving the 1906 Mw7.1 Meishan, Taiwan, earthquake from historical seismic records. Seismol Res Lett 89(4):1385–1396
Lin CR (2021) Revisiting the 1906 M 7.1 Meishan, Taiwan, Earthquake: A dynamic rupture modeling perspective on single-fault versus multi-fault, Master's thesis, Department of Earth Sicence, National Central University, Chung-Li, Taiwan
Ma KF, Chan CH, Stein RS (2005) Response of seismicity to Coulomb stress triggers and shadows of the 1999 Mw= 7.6 Chi-Chi, Taiwan, earthquake. J Geophys Res Solid Earth 110(B5)
Page MJ, McKenzie JE, Bossuyt PM, Boutron I, Hoffmann TC, Mulrow CD, Shamseer L, Tetzlaff JM, Akl EA, Brennan SE, Chou R, Glanville J, Grimshaw JM, Hróbjartsson A, Lalu MM, Li T, Loder EW, Mayo-Wilson E, McDonald S, McGuinness LA, Stewart LA, Thomas J, Tricco AC, Welch VA, Whiting P, Moher D (2021). The PRISMA 2020 statement: an updated guideline for reporting systematic reviews. Int J Surgery 88:105906
Shyu JBH, Chuang YR, Chen YL, Lee YR, Cheng CT (2016) A new on-land seismogenic structure source database from the Taiwan Earthquake Model (TEM) project for seismic hazard analysis of Taiwan. Terr Atmos Oceanic Sci 27(3):311–323
Shyu JBH, Yin YH, Chen CH, Chuang YR, Liu SC (2020) Updates to the on-land seismogenic structure source database by the Taiwan Earthquake Model (TEM) project for seismic hazard analysis of Taiwan. Terr Atmos Ocean Sci 31(4):469
Stein RS (2004) Tidal triggering caught in the act. Science 305(5688):1248–1249
Stirling MW, Zuniga FR (2017) Shape of the magnitude–frequency distribution for the Canterbury earthquake sequence from integration of seismological and geological data. Bull Seismol Soc Am 107(1):495–500
Stirling M, Goded T, Berryman K, Litchfield N (2013) Selection of earthquake scaling relationships for seismic-hazard analysis. Bull Seismol Soc Am 103(6):2993–3011
Su HY (2019) The multi-fault rupture process of 1935 Hsinchu-Taichung Earthquake, Taiwan revealed from dynamic modelling. PhD Thesis. National Central University
Toda S, Stein RS, Sevilgen V, Lin J (2011) Coulomb 3.3graphic-rich deformation and stress-change software forearthquake, tectonic, and volcano research and teaching—userguide, U.S. Geol. Surv. Open-File Rept. 2011–1060, 63 pp., Earthquake Science Center, Menlo Park Science Center, MenloPark, California
Ulrich T, Gabriel AA, Ampuero JP, Xu W (2019) Dynamic viability of the 2016 Mw 7.8 Kaikōura earthquake cascade on weak crustal faults. Nat Commun 10(1):1–16
Wang YJ, Chan CH, Lee YT, Ma KF, Shyu JBH, Rau RJ, Cheng CT (2016a) Probabilistic seismic hazard assessment for Taiwan. Terr Atmos Ocean Sci 27(3):325–340
Wang YJ, Lee YT, Chan CH, Ma KF (2016b) An investigation of the reliability of the Taiwan Earthquake Model PSHA2015. Seismol Res Lett 87(6):1287–1298
Wei S, Fielding E, Leprince S, Sladen A, Avouac JP, Helmberger D et al (2011) Superficial simplicity of the 2010 El Mayor-Cucapah earthquake of Baja California in Mexico. Nat Geosci 4(9):615–618
Wells DL, Coppersmith KJ (1994) New empirical relationships among magnitude, rupture length, rupture width, rupture area, and surface displacement. Bull Seismol Soc Am 84(4):974–1002
Yen YT, Ma KF (2011) Source-scaling relationship for M 46–89 earthquakes, specifically for earthquakes in the collision zone of Taiwan. Bull Seismol Soc Am 101(2):464–481
Yen MH, Lee SJ, Ma KF (2016) The source rupture analysis and 3-D seismic wave simulations of the 1935 Hsinchu-Taichung Earthquake. PhD Thesis. National Central University
Youngs RR, Coppersmith KJ (1985) Implications of fault slip rates and earthquake recurrence models to probabilistic seismic hazard estimates. Bull Seismol Soc Am 75(4):939–964

Publisher's Note